ACS Photonics

Article

pubs.acs.org/journal/apchd5

Synthesis and Optical Properties of Homogeneous Nanoshurikens

Judit Morla-Folch,[†] Luca Guerrini,[†,‡] Nicolas Pazos-Perez,*[,†,‡] Raul Arenal,*[,§,∥] and Ramon A. Alvarez-Puebla*[,†,‡,⊥]

[†]Departamento de Química Física e Inorgánica, Universitat Rovira i Virgili and Centro Tecnologico de la Quimica de Cataluña, Carrer de Marcel·lí Domingo s/n, 43007 Tarragona, Spain

[‡]Medcom Advance SA, Viladecans Bussines Park, Carrer de Bertran i Musitu, 83−85, 08840 Viladecans, Barcelona, Spain

[§]Laboratorio de Microscopias Avanzadas (LMA), Instituto de Nanociencia de Aragon (INA), Universidad de Zaragoza, 50018 Zaragoza, Spain

[∥]Fundacion ARAID, 50018 Zaragoza, Spain

[⊥]ICREA, Passeig Lluís Companys 23, 08010 Barcelona, Spain

Supporting Information

ABSTRACT: During the last years the controlled synthesis of Au nanoparticles (NPs) has almost become a reality, and structures such as spheres, cubes, rods, decahedra, or octahedra can be prepared with *a la carte* dimensions in a very homogeneous manner. However, the fabrication of spiked particles, the most efficient plasmonic NPs, with controllable geometric parameters remains elusive. Here we show how to prepare highly homogeneous spiked nanoparticles composed of a penta-twinned core and five tips. These nanoparticles, reminiscent of ninja nanoshurikens (throwing stars), exhibit the ability to concentrate large electromagnetic fields at the apexes of the tips upon illumination. The apexes also present high affinity for analytes, giving rise to an unprecedented capacity for quantitative optical ultradetection with SERS.

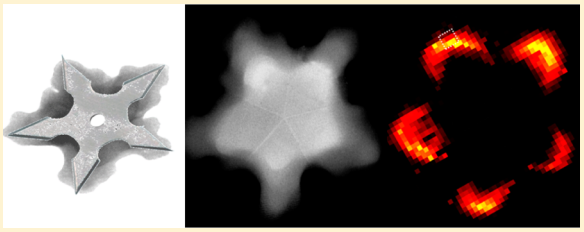

KEYWORDS: *plasmon concentration, SERS, plasmonic particles, EELS, STEM-HAADF*

The mobility of electrons in nanoparticles (NPs) of noble metals[1] leads to unusually electromagnetic responses in the UV−vis−NIR range (i.e., localized surface plasmon resonances, LSPRs). This effect makes NPs uniquely suitable for a variety of applications including detection and therapy. For gold NPs, the intriguing properties of their LSPRs are combined with low toxicity to eukaryotic cells, which has spurred multiple biomedical applications such as photoinduced hyperthermia[2] for the treatment of cancer[3] or optical diagnostics[4−6] and imaging[7,8] by surface-enhanced Raman scattering (SERS) spectroscopy. Thus, in many ways, Au NPs represent an ideal materials platform for theranostics.[9]

The optical properties of metallic NPs are strongly shape- and size-dependent.[10,11] It has been demonstrated that NPs with sharp corners such as triangles,[12] cubes,[13] rods,[14] or octahedra,[15] and tips such as nanostars,[16−19] spiked rods,[20,21] spiked octahedra,[22] or spiked beads[23,24] can highly concentrate the electric field, giving rise to a significant amplification of the SERS intensity when they are used as optical-enhancing substrates.[25] During the last years the controlled synthesis of Au NPs has almost become a reality, and structures such as spheres, cubes, rods, decahedra, or octahedra can be prepared with *a la carte* dimensions in a very homogeneous manner.[26] However, the fabrication of spiked particles, the most efficient plasmonic NPs,[25,27] with controllable geometric parameters remains elusive. Although these particles can be prepared homogeneously in size, spike growth normally results in random distribution of tip number and geometry (i.e., height, width, and aperture angle).[16] As the geometry characteristics are responsible for the degree of plasmon concentration,[25] the random growth of spikes implies that each tip, and thus each star, behaves differently upon excitation with light with the subsequent random intensification of the Raman signal. In other words, although the spiked particles are among the few structures capable of maintaining enough field enhancement to be detected as single particles, their optical response is not quantitative due to the field enhancement fluctuations associated with their uncontrolled growth.

In this article, we show that the preparation of spiked particles with homogeneous structural and optical characteristics is possible. These novel spiked gold nanoparticles are composed of a penta-twinned core and five tips. To some degree, they are reminiscent of ninja nanoshurikens in terms of shape and topology. Because of their high plasmon concentration at the tips, demonstrated through EELS mapping, these structures act as excellent substrates for optically enhanced spectroscopies such as SERS. We demonstrate that due to their particular structure, these particles induce a considerably larger enhancement than nanospheres of similar size or even nanostars, prepared with

Received: September 18, 2014
Published: October 26, 2014

   dx.doi.org/10.1021/ph500348h | *ACS Photonics* 2014, 1, 1237−1244

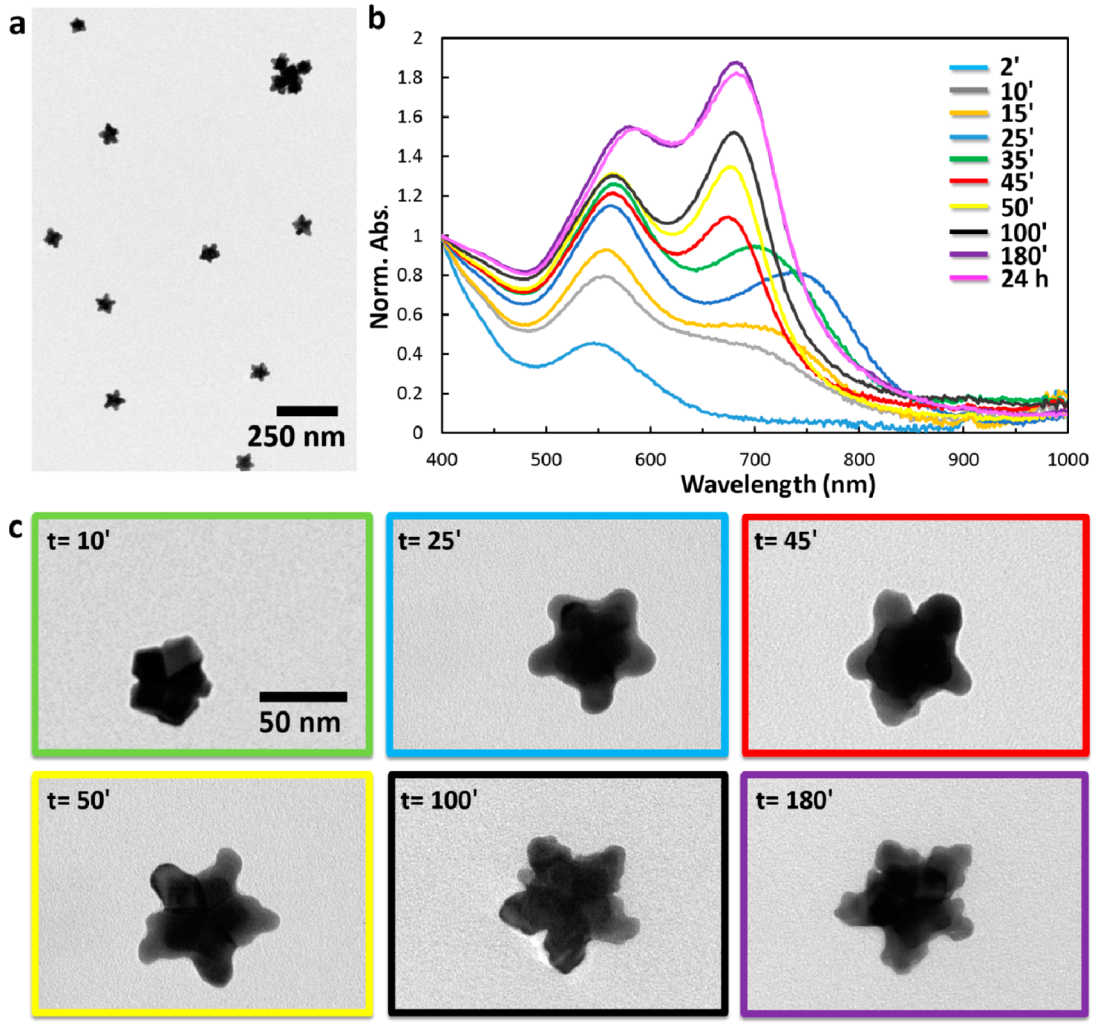

Figure 1. (a) Representative TEM image of the AuNShs after reaction completion. (b) UV−vis−NIR spectra and (TEM) images of the nanoparticles at different times during the reaction.

conventional methods, because they act as single-particle hotspots in suspension.

The synthesis of spiked gold nanocrystals can be carried out by using structurally well-defined spherical seeds. In gold nanoparticles with a well-defined multitwinned structure the most reactive (energetic) regions at the surface are the twin boundaries. These regions preferentially grow when reducing Au^{I} to Au^{0} on their surfaces.[28,29] At the beginning of the growth process, each twin boundary starts developing a spike. However, though slowly, during this process the particle also grows, generating new twin boundaries, which, in turn, result in more spikes. With the standard synthetic methods for gold nanostars,[30−32] the growth of the structures is controlled by the fast kinetics at the beginning of the reduction, hindering the possibility to control the number and geometry of the tips.[30,33] Consequently, this synthetic process ends with multispiked structures of an uncontrollable number of different tips. Thus, the careful regulation of reduction kinetics is a key factor to achieve the control of the number and geometry of tips in the spiked structure.

RESULTS AND DISCUSSION

In order to obtain highly homogeneous five-tipped nanostars (i.e., nanoshurikens, AuNShs), two main parameters were considered: control over reduction kinetics and seed crystallinity.

The reduction kinetics of the growing reaction is influenced mainly by (i) the temperature, (ii) the reducing agent, and (iii) the water content. In most of the synthetic protocols, temperature plays a crucial role in determining the final morphology and size of the nanoparticles, as lowering the temperature normally slows the growth kinetics.[34] However, in the case of standard gold nanostars (AuNSt), the temperature affects only the final properties of the product when raised above 60 °C by inducing a reshaping of the stars into spheres. For lower temperatures, the reaction yields nanostars with no evidence of any modification.[30] We then focused our attention on the second parameter, the reducing agent. Classically, the reduction of gold to yield nanostars is carried out in *N*,*N*-dimethylformamide (DMF)[35] in the presence of polyvinylpyrrolidone (PVP).[30] It is known that the PVP concentration strongly influences the reduction kinetics.[30] At low concentrations, PVP does not reduce Au^{I}, whereas high concentrations promote a rapid reduction. Importantly, DMF does not act merely as a solvent, but also increases the reduction capacity of PVP by solubilizing the polymer.[32] With all these considerations in mind, we designed a synthesis at 25 °C where DMF is replaced by ethanol as a solvent, and a relatively high polymer

dx.doi.org/10.1021/ph500348h | ACS Photonics 2014, 1, 1237−1244

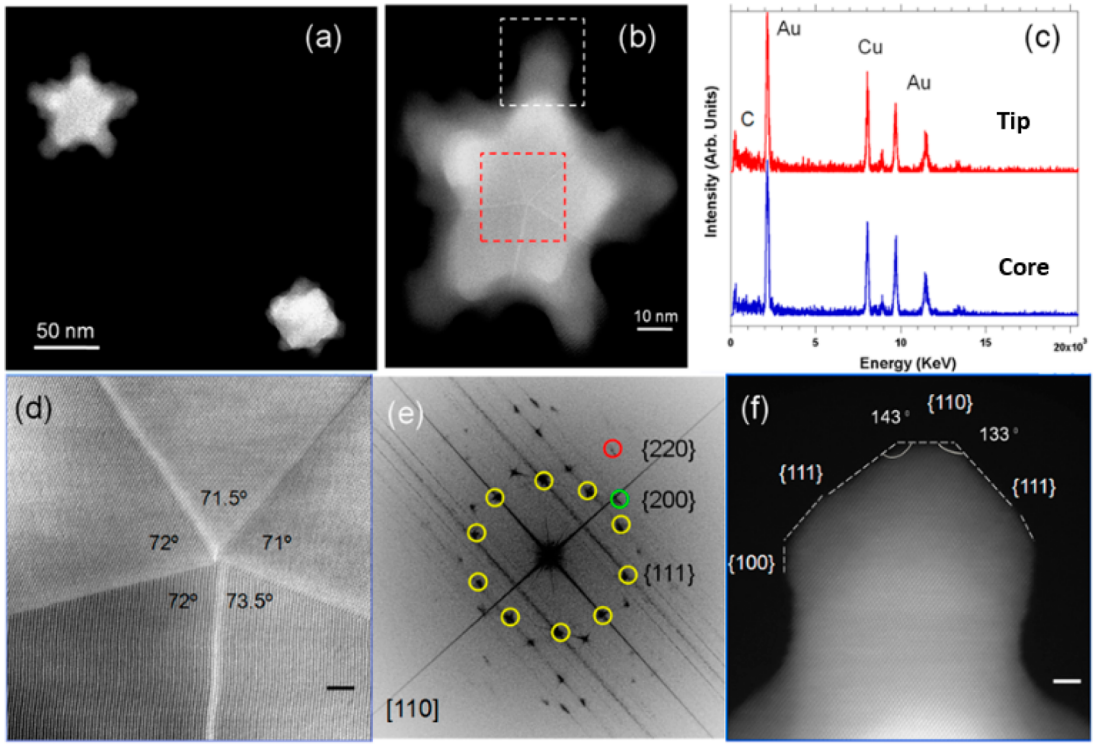

Figure 2. (a) Low-magnification HAADF-STEM image of AuNShs differently oriented with respect to the carbon support film, respectively. (b) Medium-magnification HAAD-STEM image of one of these AuNShs, consisting of a 5-fold star structure composed of a decahedral core and five tips. (c) EDS spectra recorded at the core and at the tip, marked by the red and white squares, respectively. Carbon, copper (both elements come from the TEM grid), and gold are visible in the EDS spectra. (d) HAADF HRSTEM micrograph of the core of the nanoparticle showing its decahedral structure. The 5-fold symmetry and the multiple twinning domains are clearly evidenced. (e) FFT obtained from the red square marked area of (b) (equivalent to (c)). For the sake of clarity, the color of this FFT is inverted. The superimposed contribution of each of the crystals composing the decahedral core, rotated with respect to each other, of the {111}, {200}, and {220} planes, is marked with yellow, green, and red, respectively. (f) HAADF image of the tip marked by a white square in (b).

concentration is employed (5 mM, PVP_{k58}). Because ethanol is less polar than DMF, it decreases the solubility of PVP and thus slows the reaction rate. As particle seeds, we selected multitwinned nanoparticles of 15 nm diameter obtained through a modification of the well-known Turkevich method, using citrate as capping and reducing agent.[26,36−38] These nanoparticles show well-defined crystallinity with crystal facets formed by {111} planes (Figure S1).

Figure 1a shows a representative TEM image of the obtained products (i.e., AuNShs) after 3 h of reaction. Note that common gold nanostar synthesis is finished in 30 min.[39] AuNShs are characterized by a narrow distribution of both overall size and tip length (Figure S2). The monitoring of the reaction process by UV−vis−NIR spectroscopy (Figure 1b) and TEM (Figure 1c) reveals that the plasmonic band related to the tips starts appearing around 700 nm (after approximately 10 min) and red-shifts to 760 nm within 25 min. After this time, the tip-plasmon band blue-shifts to 685 nm as a consequence of the reshaping of the tips. Interestingly, the plasmon of the core initially centered at 545 nm red-shifts to 580 nm in the AuNSh. Although a slight growth of the core can be observed in the TEM images, this does not justify such a drastic spectral change. Thus, the shift can be better interpreted as a retardation effect due to the growth of tips, which hinders the movement of electrons in the nanostructure core. Remarkably, the TEM images clearly indicate how the drastic slowing of the kinetics at the beginning of the reduction promotes the conversion of the multi-twinned seeds into well-defined penta-twinned structures (Figure 1a, t = 10 min). Based on the studies reported in the literature,[40−43] we cannot discard that the initial crystallinity of the PVP-coated gold seeds could have been improved by thermal treatment during their transfer to DMF at 60 °C at 90 mbar for 1 h. However, HRTEM analysis of the seeds before and after the transfer to DMF did not show appreciable changes.

It is worthy to note that the reaction should be carried out in anhydrous conditions (i.e., the role of water content). In fact, due to the lower polarity of ethanol as compared with DMF, the presence of water content even at minute concentrations increases the reaction rate by solubilizing more PVP. This fact has been experimentally observed by a faster color change of the solution when water was added. Moreover, as the content of water increases, the band related to the spikes becomes less intense, indicating the formation of more rounded particles (Figure S3).

Structural characteristics of our AuNSh were studied by high-resolution scanning transmission electron microscopy (HR-STEM). Figure 2a shows a low-magnification high-angle annular dark-field (HAADF) scanning transmission electron microscopy image of two AuNShs. Although the shape of these nanoparticles seems to be different, this is due to their different orientation with respect to the supporting carbon film. A close look at a single AuNSh reveals a structure consisting of a decahedral core with five tips, which grow symmetrically from each corner of the central decahedron (Figure 2b,d). However, the relaxation mechanism for their stabilization is still to be

dx.doi.org/10.1021/ph500348h | ACS Photonics 2014, 1, 1237−1244

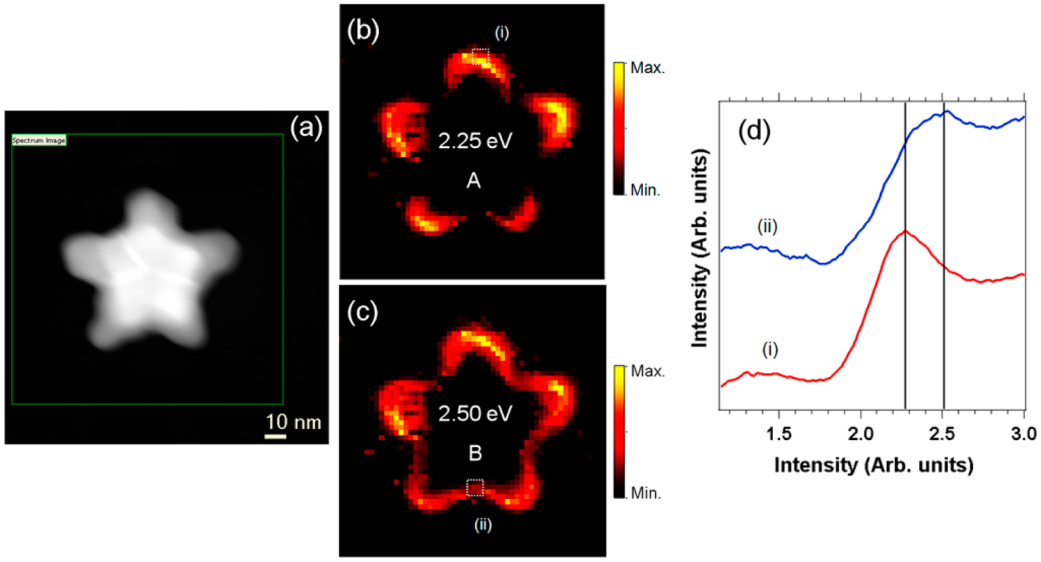

Figure 3. (a) HAADF-STEM of a AuNSh. EELS spectrum-imaging has been recorded in the square area marked in green. (b and c) Intensity maps extracted from the EELS spectrum-imaging after removing the zero-loss peak. The intensity maps show the spatial distribution of the two excited LSPR modes of the AuNSh, noted as A and B. (d) EELS spectra (each of them corresponds to the sum of 9 spectra) extracted from the EELS spectrum-imaging in the areas marked in each of the intensity maps (square regions) and marked as (i) and (ii), respectively.

elucidated. X-ray energy-dispersive spectroscopy (EDS) recorded at different areas (Figure 2c) confirms that AuNShs are composed exclusively by pure gold. The copper and carbon contribution observed in the spectra correspond to the contribution of the supporting TEM grid. The image illustrated in Figure 2d was acquired at the core of the AuNSh and shows twinning boundaries coherent and free of defects such as dislocation or microtwinning. The angles among the adjacent boundaries are displayed in the micrograph and vary from 71.0° to 73.5°. In an ideal regular decahedron, the particle is constructed from five tetrahedral domains rotated around a shared central axis (angles 70.52°) and contains a disclination of power of −7.4°.[44] However, all real materials exhibit some degree of anisotropy and real decahedral particles are not simple geometric shapes.[45] Indeed, the morphology and structure of these nanomaterials are even more complicated, as they are composed of two geometrical elements: the core and tips. This fact can justify the slight deviation from the ideal decahedral structure. In this sense, it is interesting to analyze the fast Fourier transform (FFT) of the Au nanoparticle obtained from the decahedral core (Figure 2e). This complex set of spots can be well interpreted by the superposition of five subcrystals related to face-centered cubic gold crystals with a [110] orientation, and each spot can be simply attributed to a specific subcrystal.[46] Thus, as the decahedron is formed by five tetrahedra with twin-related adjoining faces, by superimposing the [110] direction contribution of each crystal rotated with respect to each other, the 5-fold-symmetry FFT of Figure 2e can be generated. The different contribution of each set of planes is also marked in this figure. Finally, the structure of the tips is also analyzed in Figure 2f. The tips are highly crystalline with apex-exposing {110} facets at the center and apex {111} facets at the sides. This crystallography is of key importance, as previously reported results indicate that {110} facets react very strongly with thiols,[47] generating preferential absorption over other facets such as {111} or {100}.[48,49]

In order to investigate locally the optical properties of the AuNShs, high-energy resolution (monochromated) electron energy loss spectroscopy (EELS) was carried out.[12,16,50−53] Figure 3a shows an HAADF image acquired in AuNSh where the EELS analysis was carried out. Figure 3b and c show the EELS spectrum-imaging[54,55] low-loss region (below 50 eV) after zero-loss peak subtraction with the corresponding EEL spectra extracted from the areas marked by white (Figure 3d). The analysis of the two LSPR features reveals that the AuNSh displays two distinct azimuthal dipolar bright SP modes, involving collective conduction−electron oscillations and induced dipoles along the 5-fold symmetry axis.[56] One of them is localized at the tips at 2.25 eV (551 nm) and the other at 2.5 eV (495 nm), corresponding to the core with some contribution of the tips (Figure S4 shows the EELS spectrum of the gold seeds). Both bands correlates well with previous studies on gold nanostars.[16] Notably, both LSPRs are blue-shifted with respect to those recorded in solution (at 685 and 580 nm for the tip and core localized plasmons, respectively). However, this can be explained in terms of the completely different dielectric environment for both measurements, including the TEM support and the vacuum for EELS, and the surfactant and the solvent for the UV−vis−NIR.

In order to test the SERS activity of the AuNShs, thiophenol (TP) was used as a Raman probe. TP is a well-known analyte, with its HOMO−LUMO band far away in the blue spectral region; thus no chemical effects are expected to occur under the employed 785 nm laser excitation.[57] Results were compared with those obtained with standard gold nanostars (AuNSts) of similar size and spherical gold citrate nanoparticles of approximately 55 nm in diameter (see Figure S5). To avoid biased results due to uncontrolled aggregation of nanoparticles upon TP functionalization, the colloids were previously passivated with Tween 20 (polyethylene glycol sorbitanmonolaureate), a nonionic surfactant that physisorbes on gold surfaces, and then transferred to water. Tween 20 is commonly used in gold nanoparticle surface modification by chemisorption of thiolated molecules[58−60] to provide an effective steric protection that hampers irreversible aggregation. Intense TP features arise in the SERS spectrum[61] on AuNShs using a near-

dx.doi.org/10.1021/ph500348h | ACS Photonics 2014, 1, 1237−1244

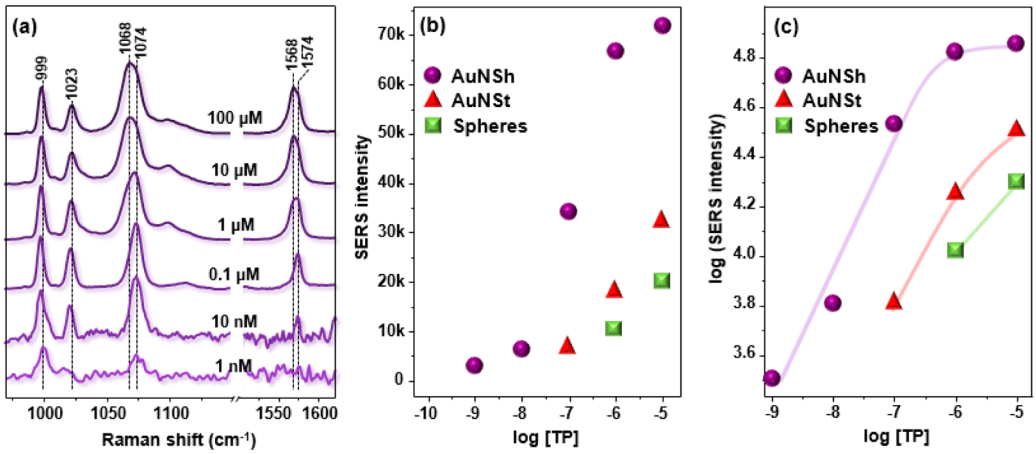

Figure 4. (A) Normalized and baseline-corrected SERS spectra in the 970−1170 cm^{-1} and 1500−1650 cm^{-1} spectral ranges of TP at different concentrations on Tween 20-stabilized AuNSh colloids. In this case, the signal background (Figure S7) was digitally subtracted to remove spurious bands. The spectra were acquired at 785 nm using a long-working-distance objective. (B and C) SERS intensity of the 1074 cm^{-1} TP band (linear and logarithmic scale) at different concentrations obtained on Tween 20-stabilized nanoparticles (AuNShs, AuNSts, and Au spherical colloids) under the same experimental conditions (785 nm, 10% laser power, 10 s exposure, 2 accumulations, and [Au^0] = 0.173 mM).

infrared 785 nm excitation source (Figure 4a). Among others, the spectrum is characterized by bands at 1574 cm^{-1}, attributed to the aromatic ν(CC) modes, at 1074 cm^{-1}, ascribed to a ring breathing mode coupled with ν(CS), and at 1023 and 999 cm^{-1}, both resulting from ring breathings vibrations. In contrast, no TP bands were observed when the same sample was illuminated with a 633 nm laser line (Figure S6). It is worth noticing that the SERS spectrum of Tween 20-modified AuNSh was acquired as a background signal (Figure S7) and removed from the SERS spectra of TP by digital subtraction. Figure 4a illustrates the normalized SERS spectra of TP on Tween 20-stabilized AuNSh and AuNSt aqueous suspensions (both [Au^0] = 0.173 mM) in the ring breathing and C═C spectral regions obtained at different Raman probes. The SERS spectra show that TP features can be clearly distinguished down to the nanomolar level. Interestingly, a significant alteration in the Raman probe spectral profile takes place when the TP concentration is progressively raised (Figure 4a and Figure S8). Among others, we highlight the remarkable shifts from 1574 to 1568 cm^{-1} of the ν(CC) band and from 1074 to 1068 cm^{-1} of the combined ring breathing + ν(CS) mode. Such spectral reshaping is not observed for 55 nm nanospheres (Figure S9), suggesting that TP molecules do not undergo a significant structural rearrangement when the surface crowding is progressively increased up to the full coverage and lateral interactions are expected to take place. Thus, the vibrational signatures of the TP appearing in the SERS spectra must be associated with different chemisorption sites available on the gold surface.[62] At low concentrations, the TP tends to interact preferably with {110} facets.[47−49] In AuNShs, these facets are placed at the apexes of the tips, where most of the electric field is accumulated upon plasmon excitation. Further, by illuminating the samples with a 785 nm laser line, the excitation is to the red of the bulk plasmon resonance and the main component of the field is the one normal to the surface.[63] Thus, in the case of the molecules chemisorbed at the planar apex of the tip, the excitation of their vibrational modes is directly perpendicular to the surface, with the subsequent further enhancement of the those modes parallel to this surface vector (1574 and 1074 cm^{-1}), in agreement with the surface selection rules.[64] As the amount of TP increases, other facets become available including the {100} and the {111}. Notably, the anisotropic plasmonic nature in these structures makes their contribution to the enhancement of those chemisorbed molecules less pronounced in terms of both the absolute enhancement, as the field is weaker, and relative enhancement of the different bands, as the molecules are not placed in the facet where the major electromagnetic contribution is that normal to the surface. This effect cannot be observed in both isotropic spherical particles (Figure S9), as the plasmon contribution is symmetric through the entire surface (especially for particles in movement, as in the case of colloidal solutions), and highly anisotropic standard gold nanostars (Figure S10). To quantitatively compare the SERS efficiency of AuNShs to those of AuNSts and spheres, we plotted the SERS intensities of the TP band at approximately 1073 cm^{-1} against the TP concentration in Figure 4b and c (linear and logarithmic scale, respectively). The SERS spectra were obtained at 785 nm (10% laser power, 10 s exposure, 2 accumulation) under a constant Au^0 concentration (0.173 mM). The corresponding SERS efficiencies under these experimental conditions were then estimated. As can be seen, the AuNShs present a remarkably higher enhancement factor (EF) of 5×10^6 over AuNSt (1×10^6) or spherical particles (4×10^5). Further, and due to the high similarity between the tips together with the high affinity of the gold apexes for the analyte, the detection is linearly quantitative especially at minute concentrations of TP.

CONCLUSIONS

In summary, here we illustrate how to prepare highly homogeneous complex nanoparticles with the ability to concentrate large electromagnetic fields in certain regions of their surface upon illumination with the appropriate light. These particles, reminiscent of ninja shurikens, present a high affinity for analytes in these hot optical areas (at the apexes of the tips). The high homogeneity of the tips in between the same and different particles, giving rise to an unprecedented capacity for quantitative optical ultradetection with SERS, paves the way for the design of new single-particle optical sensors with applications in biology, medicine, and environmental sciences.

dx.doi.org/10.1021/ph500348h | ACS Photonics 2014, 1, 1237−1244

METHODS

Materials. Gold(III) chloride trihydrate (99.9°%, $HAuCl_4 \cdot 3H_2O$), polyvinylpyrrolidone (PVP, MW 58000), trisodium citrate dihydrated (99.9°%), Tween 20, thiophenol, ethanol (99.5%), and *N*,*N*-dimethylformamide (DMF, 99.9%) were purchased from Sigma-Aldrich (Germany). All reactants were used without further purification. Milli-Q water (18 MΩ cm^{-1}) was used in all aqueous solutions, and all the glassware was cleaned with aqua regia before the experiments.

Synthesis of Spherical Gold Seeds. Spherical multitwinned gold nanoparticles of 15 nm diameter were produced by a modification of the well-known Turkevich method.[36,37] Briefly, the Au particles were prepared by adding 347 μL of a 0.12 M $HAuCl_4$ solution into a boiling aqueous solution containing 250 mL of 2.2 mM sodium citrate under vigorous stirring, using a condenser to prevent the evaporation of the solvent. The mixture was allowed to react for 1 h while boiling and under continuous stirring. During this time, the color of the solution changed gradually from colorless to purple and finally acquired a deep red color.

Transfer and Concentration of the Spherical Gold Seeds. The 15 nm Au particles were transferred into DMF using a modification of the method previously reported by Graff et al.[65] The as-prepared gold nanoparticles (100 mL) were added dropwise under vigorous stirring to a PVP solution in DMF (40 mL, 5.6 mM). To guarantee that PVP adsorption on the gold nanoparticle surface was complete, the reaction mixture was allowed to stir for 24 h at room temperature. Finally, a rotary evaporation was used to remove the water content from the mixture as well as to concentrate the nanoparticles. The colloidal suspension was allowed to stand for 1 h at 60 °C and 90 mbar until a volume of 15 mL was left in the flask (final Au^0 concentration = 4.025 mM).

The 15 nm Au particles were also transferred into ethanol using PVP as a phase transfer agent.[65] The as-prepared gold nanoparticles (150 mL) were added dropwise under vigorous stirring to a PVP solution in ethanol (40 mL, 5.6 mM). To guarantee that PVP adsorption on the gold nanoparticle surface was complete, the reaction mixture was allowed to stir for 24 h at room temperature. To transfer the PVP-stabilized particles into ethanol, the solution was centrifuged (10 000 rpm, 30 min), the supernatant was removed, and the particles were redispersed in ethanol (all in 20 mL). Final Au^0 concentration was 0.6 mM.

Synthesis of Gold Nanoshurikens. Nanoshurikens of approximately 75 nm were prepared by adding 15 nm PVP-coated gold seeds in DMF to a mixture of $HAuCl_4$ and PVP in EtOH. A 5 mM solution of PVP in EtOH (10 mL) was prepared. Next, 41.7 μL of an aqueous solution of $HAuCl_4$ (0.12 M) was added. After 30 s, 80 μL of the Au seeds (final Au concentration was 1.654 mM) was injected under vigorous stirring. Within 45 min, the color of the solution changed from pink to blue, indicating the formation of AuNShs. However, the solution was left under stirring overnight to ensure the complete reduction of the $HAuCl_4$.

Synthesis of Quasi-spherical Gold Colloids of 55 nm. Large gold nanoparticles of approximately 55 nm diameter were prepared by following the previously reported seeded growth method.[66] Briefly, 125 mL of a solution of $HAuCl_4$trihydrate (14.57 mg) in Milli-Q water was heated to boiling; then, under vigorous stirring, 3.75 mL of Au seeds and 2.56 mL of an aqueous solution of trisodium citrate (1% w/w) were consecutively added to the solution. The mixture was refluxed for 30 min before adding 4.3 mL of a 4.6% w/w trisodium citrate aqueous solution. The solution was finally allowed to boil for another hour and allowed to cool to room temperature under gentle stirring for several hours.

Synthesis of Conventional Gold Nanostars. Nanostars of approximately 70 nm were prepared by sonicating for 15 min a solution of PVP (15 mM) in DMF (35 mL). To the mixture was added $HAuCl_4$ (162 μL, 0.108 M) under rapid stirring at room temperature, followed by the rapid addition of 15 nm PVP-coated gold seeds in ethanol (1764 μL, 0.6 mM). Within 20 min, the color of the solution changed from pink to blue, indicating the formation of AuNSt. Excess PVP was removed by 5-fold centrifugation (7000 rpm) and dispersed in ethanol.

Characterization. UV−vis spectroscopy (Thermo Scientific Evolution 201) and transmission electron microscopy (TEM, JEOL 1011 operating at 100 kV) were applied to characterize the optical response and size of the nanoparticles. TEM samples were prepared by drying ethanoic suspensions on carbon-Formvar-coated 200-mesh copper grids.

High-Resolution STEM, EDS, and EELS Analyses. TEM samples were prepared placing a drop of the nanoparticle aqueous suspension directly on a copper carbon holey grid that was left drying in air before putting it inside the microscope. All the HRSTEM studies (EDS, imaging, and EELS) were performed using a FEI Titan low-base microscope, working at 300 kV. This microscope is equipped with a Cs probe corrector, a monochromator, and ultrabright X-FEG electron source. The spectra were collected in STEM mode, using spectrum-image mode.[54,55] In the case of low-loss EELS, 15 spectra (of 4 ms each) were acquired for each probe position following a 2D region across the nano-object. It is worth noting that no evidence of irradiation damage in the samples was detected during the EEL spectra acquisition. The convergence and collection angles were 25 and 35 mrad, respectively, and the energy resolution was ∼200 meV. The tail of the zero-loss peak has been removed using a power law subtraction method.[67]

Surface-Enhanced Raman Scattering Spectroscopy. Excess PVP was removed by 8-fold centrifugation (7000 rpm, 20 min) and redispersion in EtOH. In order to be characterized by SERS, the AuNShs were transferred to water. Tween 20 (15% in ethanol) was added, and the solution was agitated for 1 h to maintain the particle stability and to avoid aggregation during the transfer. The samples were again centrifuged (5000 rpm, 15 min), redispersed with an aqueous solution of Tween 20 (15%), and left under stirring for 1 h. Subsequently, a final centrifugation step was performed (5000 rpm, 15 min), and the sediment was redispersed in ultrapure water (2 mL); the final Au concentration was 0.173 mM. Finally, 100 μL of these colloids was functionalized with 5 μL of thiophenol ethanolic solutions at different concentrations, yielding final Raman probe concentrations in the 10^{-5} to 10^{-10} M range. The samples were left overnight under gentle shaking before the SERS measurements were acquired. An identical protocol was applied to standard gold nanostars. In the case of gold nanospheres, the colloids are already dispersed in water, and thus the initial step of transfer from the ethanolic solution to the aqueous one was no longer necessary. Therefore, the Tween 20 functionalization was directly performed in the original colloidal medium. The SERS characterization of AuNSt and 55 nm diameter gold nanospheres were performed under the identical experimental conditions to those for AuNShs (Au concentration, laser power, and exposure time). SERS experi-

ments were conducted using a Renishaw InVia Reflex confocal microscope equipped with a high-resolution grating consisting of 1200 grooves/cm for NIR wavelengths (785 nm), additional band-pass filter optics, and a 2D-CCD camera. The measurements were performed with a macrosampling objective with acquisition times of 10 s and 20 mW of power at the sample.

■ ASSOCIATED CONTENT

Supporting Information

Additional nanoparticle characterization including UV−vis−NIR, SERS spectroscopies, and TEM. This material is available free of charge via the Internet at http://pubs.acs.org.

■ AUTHOR INFORMATION

Corresponding Authors

*E-mail: npazos@medcomadvace.com.
*E-mail: arenal@unizar.es.
*E-mail: ramon.alvarez@urv.cat.

Notes

The authors declare no competing financial interest.

■ ACKNOWLEDGMENTS

The research leading to these results has received funding from the European Union Seventh Framework Program under the following grant agreements: FP7MC-IEF329131 (CrossSERS); FP7MC-IEF-623527 (PRIOSERS) and 312483 - ESTEEM2 (Integrated Infrastructure Initiative−I3).This work was also funded by the Spanish Ministerio de Economia y Competitividad (CTQ2011-23167 and FIS2013-46159-C3-3-478 P) and Medcom Advance SA. The TEM measurements were performed in the Laboratorio de Microscopias Avanzadas (LMA) at the Instituto de Nanociencia de Aragon (IN-A)−Universidad de Zaragoza.

■ REFERENCES

(1) Lu, X.; Rycenga, M.; Skrabalak, S. E.; Wiley, B.; Xia, Y. Chemical Synthesis of Novel Plasmonic Nanoparticles. *Annu. Rev. Phys. Chem.* **2009**, *60*, 167−192.

(2) Sperling, R. A.; Rivera Gil, P.; Zhang, F.; Zanella, M.; Parak, W. J. Biological Applications of Gold Nanoparticles. *Chem. Soc. Rev.* **2008**, *37*, 1896−1908.

(3) Boyer, D.; Tamarat, P.; Maali, A.; Lounis, B.; Orrit, M. Photothermal Imaging of Nanometer-Sized Metal Particles among Scatterers. *Science* **2002**, *297*, 1160−1163.

(4) Qian, X.; Peng, X.-H.; Ansari, D. O.; Yin-Goen, Q.; Chen, G. Z.; Shin, D. M.; Yang, L.; Young, A. N.; Wang, M. D.; Nie, S. In Vivo Tumor Targeting and Spectroscopic Detection with Surface-Enhanced Raman Nanoparticle Tags. *Nat. Biotechnol.* **2008**, *26*, 83−90.

(5) Alvarez-Puebla, R. A.; Liz-Marzan, L. M. SERS-Based Diagnosis and Biodetection. *Small* **2010**, *6*, 604−610.

(6) Alvarez-Puebla, R. A.; Zubarev, E. R.; Kotov, N. A.; Liz-Marzán, L. M. Self-Assembled Nanorod Supercrystals for Ultrasensitive SERS Diagnostics. *Nano Today* **2012**, *7*, 6−9.

(7) Ando, J.; Fujita, K.; Smith, N. I.; Kawata, S. Dynamic SERS Imaging of Cellular Transport Pathways with Endocytosed Gold Nanoparticles. *Nano Lett.* **2011**, *11*, 5344−5348.

(8) Rivera_Gil, P.; Vazquez-Vazquez, C.; Giannini, V.; Callao, M. P.; Parak, W. J.; Correa-Duarte, M. A.; Alvarez-Puebla, R. A. Plasmonic Nanoprobes for Real-Time Optical Monitoring of Nitric Oxide inside Living Cells. *Angew. Chem., Int. Ed.* **2013**, *52*, 13694−13698.

(9) Kelkar, S. S.; Reineke, T. M. Theranostics: Combining Imaging and Therapy. *Bioconjugate Chem.* **2011**, *22*, 1879−1903.

(10) Halas, N. J.; Lal, S.; Chang, W.-S.; Link, S.; Nordlander, P. Plasmons in Strongly Coupled Metallic Nanostructures. *Chem. Rev.* **2011**, *111*, 3913−3961.

(11) Myroshnychenko, V.; Rodriguez-Fernandez, J.; Pastoriza-Santos, I.; Funston, A. M.; Novo, C.; Mulvaney, P.; Liz-Marzan, L. M.; Garcia de Abajo, F. J. Modelling the Optical Response of Gold Nanoparticles. *Chem. Soc. Rev.* **2008**, *37*, 1792−1805.

(12) Nelayah, J.; Kociak, M.; Stephan, O.; Garcia de Abajo, F. J.; Tence, M.; Henrard, L.; Taverna, D.; Pastoriza-Santos, I.; Liz-Marzan, L. M.; Colliex, C. Mapping Surface Plasmons on a Single Metallic Nanoparticle. *Nat. Phys.* **2007**, *3*, 348−353.

(13) Rycenga, M.; Xia, X.; Moran, C. H.; Zhou, F.; Qin, D.; Li, Z.-Y.; Xia, Y. Generation of Hot Spots with Silver Nanocubes for Single-Molecule Detection by Surface-Enhanced Raman Scattering. *Angew. Chem., Int. Ed.* **2011**, *50*, 5473−5477.

(14) Lee, S. J.; Moskovits, M. Remote Sensing by Plasmonic Transport. *J. Am. Chem. Soc.* **2012**, *134*, 11384−11387.

(15) Zhang, J.; Gao, Y.; Alvarez-Puebla, R. A.; Buriak, J. M.; Fenniri, H. Synthesis and SERS Properties of Nanocrystalline Gold Octahedra Generated from Thermal Decomposition of Haucl4 in Block Copolymers. *Adv. Mater.* **2006**, *18*, 3233−3237.

(16) Rodríguez-Lorenzo, L.; Alvarez-Puebla, R. A.; Pastoriza-Santos, I.; Mazzucco, S.; Stéphan, O.; Kociak, M.; Liz-Marzán, L. M.; García de Abajo, F. J. Zeptomol Detection through Controlled Ultrasensitive Surface-Enhanced Raman Scattering. *J. Am. Chem. Soc.* **2009**, *131*, 4616−4618.

(17) Liao, H.-G.; Jiang, Y.-X.; Zhou, Z.-Y.; Chen, S.-P.; Sun, S.-G. Shape-Controlled Synthesis of Gold Nanoparticles in Deep Eutectic Solvents for Studies of Structure−Functionality Relationships in Electrocatalysis. *Angew. Chem., Int. Ed.* **2008**, *47*, 9100−9103.

(18) Wu, H.-L.; Chen, C.-H.; Huang, M. H. Seed-Mediated Synthesis of Branched Gold Nanocrystals Derived from the Side Growth of Pentagonal Bipyramids and the Formation of Gold Nanostars. *Chem. Mater.* **2008**, *21*, 110−114.

(19) Liu, X.-L.; Wang, J.-H.; Liang, S.; Yang, D.-J.; Nan, F.; Ding, S.-J.; Zhou, L.; Hao, Z.-H.; Wang, Q.-Q. Tuning Plasmon Resonance of Gold Nanostars for Enhancements of Nonlinear Optical Response and Raman Scattering. *J. Phys. Chem. C* **2014**, *118*, 9659−9664.

(20) Pazos-Pérez, N.; Barbosa, S.; Rodríguez-Lorenzo, L.; Aldeanueva-Potel, P.; Pérez-Juste, J.; Pastoriza-Santos, I.; Alvarez-Puebla, R. A.; Liz-Marzán, L. M. Growth of Sharp Tips on Gold Nanowires Leads to Increased Surface-Enhanced Raman Scattering Activity. *J. Phys. Chem. Lett.* **2009**, *1*, 24−27.

(21) Vigderman, L.; Zubarev, E. R. Starfruit-Shaped Gold Nanorods and Nanowires: Synthesis and SERS Characterization. *Langmuir* **2012**, *28*, 9034−9040.

(22) Pedireddy, S.; Li, A.; Bosman, M.; Phang, I. Y.; Li, S.; Ling, X. Y. Synthesis of Spiky Ag−Au Octahedral Nanoparticles and Their Tunable Optical Properties. *J. Phys. Chem. C* **2013**, *117*, 16640−16649.

(23) Aldeanueva-Potel, P.; Carbó-Argibay, E.; Pazos-Pérez, N.; Barbosa, S.; Pastoriza-Santos, I.; Alvarez-Puebla, R. A.; Liz-Marzán, L. M. Spiked Gold Beads as Substrates for Single-Particle SERS. *ChemPhysChem* **2012**, *13*, 2561−2565.

(24) Liu, Z.; Yang, Z.; Peng, B.; Cao, C.; Zhang, C.; You, H.; Xiong, Q.; Li, Z.; Fang, J. Highly Sensitive, Uniform, and Reproducible Surface-Enhanced Raman Spectroscopy from Hollow Au-Ag Alloy Nanourchins. *Adv. Mater.* **2014**, *26*, 2431−2439.

(25) Alvarez-Puebla, R.; Liz-Marzán, L. M.; García de Abajo, F. J. Light Concentration at the Nanometer Scale. *J. Phys. Chem. Lett.* **2010**, *1*, 2428−2434.

(26) Grzelczak, M.; Perez-Juste, J.; Mulvaney, P.; Liz-Marzan, L. M. Shape Control in Gold Nanoparticle Synthesis. *Chem. Soc. Rev.* **2008**, *37*, 1783−1791.

(27) Solís, D. M.; Taboada, J. M.; Obelleiro, F.; Liz-Marzán, L. M.; García de Abajo, F. J. Toward Ultimate Nanoplasmonics Modeling. *ACS Nano* **2014**, *8*, 7559−7570.

(28) Wu, F.; Wen, H. M.; Lavernia, E. J.; Narayan, J.; Zhu, Y. T. Twin Intersection Mechanisms in Nanocrystalline Fcc Metals. *Mater. Sci. Eng., A* **2013**, *585*, 292−296.

(29) Zhu, Y. T.; Wu, X. L.; Liao, X. Z.; Narayan, J.; Kecskés, L. J.; Mathaudhu, S. N. Dislocation−Twin Interactions in Nanocrystalline Fcc Metals. *Acta Mater.* **2011**, *59*, 812−821.

(30) Barbosa, S.; Agrawal, A.; Rodriguez-Lorenzo, L.; Pastoriza-Santos, I.; Alvarez-Puebla, R. A.; Kornowski, A.; Weller, H.; Liz-Marzan, L. M. Tuning Size and Sensing Properties in Colloidal Gold Nanostars. *Langmuir* **2010**, *26*, 14943−14950.
(31) Khoury, C. G.; Vo-Dinh, T. Gold Nanostars for Surface-Enhanced Raman Scattering: Synthesis, Characterization and Optimization. *J. Phys. Chem. C* **2008**, *112*, 18849−18859.
(32) Senthil Kumar, P.; Pastoriza-Santos, I.; Rodriguez-Gonzalez, B.; Garcia de Abajo, F. J.; Liz-Marzan, L. M. High-Yield Synthesis and Optical Response of Gold Nanostars. *Nanotechnology* **2008**, *19*, 015606.
(33) Khoury, C. G.; Vo-Dinh, T. Gold Nanostars for Surface-Enhanced Raman Scattering: Synthesis, Characterization and Optimization. *J. Phys. Chem. C* **2008**, *2008*, 18849−18859.
(34) Plascencia-Villa, G.; Bahena, D.; Rodriguez, A. R.; Ponce, A.; Jose-Yacaman, M. Advanced Microscopy of Star-Shaped Gold Nanoparticles and Their Adsorption-Uptake by Macrophages. *Metallomics* **2013**, *5*, 242−250.
(35) Pastoriza-Santos, I.; Liz-Marzán, L. M. N,N-Dimethylformamide as a Reaction Medium for Metal Nanoparticle Synthesis. *Adv. Funct. Mater.* **2009**, *19*, 679−688.
(36) Turkevich, J.; Stevenson, P. C.; Hillier, J. A Study of the Nucleation and Growth Processes in the Synthesis of Colloidal Gold. *Discuss. Faraday Soc.* **1951**, *11*, 55−75.
(37) Enustun, B. V.; Turkevich, J. Coagulation of Colloidal Gold. *J. Am. Chem. Soc.* **1963**, *85*, 3317−3328.
(38) Johnson, C. J.; Dujardin, E.; Davis, S. A.; Murphy, C. J.; Mann, S. Growth and Form of Gold Nanorods Prepared by Seed-Mediated, Surfactant-Directed Synthesis. *J. Mater. Chem.* **2002**, *12*, 1765−1770.
(39) Khoury, C. G.; Vo-Dinh, T. Gold Nanostars for Surface-Enhanced Raman Scattering: Synthesis, Characterization and Optimization. *J. Phys. Chem. C* **2008**, *112*, 18849−18859.
(40) Liu, Y.; Mills, E. N.; Composto, R. J. Tuning Optical Properties of Gold Nanorods in Polymer Films through Thermal Reshaping. *J. Mater. Chem.* **2009**, *19*, 2704−2709.
(41) Mohamed, M. B.; Ismail, K. Z.; Link, S.; El-Sayed, M. A. Thermal Reshaping of Gold Nanorods in Micelles. *J. Phys. Chem. B* **1998**, *102*, 9370−9374.
(42) Prasad, B. L. V.; Stoeva, S. I.; Sorensen, C. M.; Klabunde, K. J. Digestive-Ripening Agents for Gold Nanoparticles: Alternatives to Thiols. *Chem. Mater.* **2003**, *15*, 935−942.
(43) Sahu, P.; Prasad, B. L. V. Time and Temperature Effects on the Digestive Ripening of Gold Nanoparticles: Is There a Crossover from Digestive Ripening to Ostwald Ripening? *Langmuir* **2014**, *30*, 10143−10150.
(44) Polonsky, I. A.; Romanov, A. E.; Gryaznov, V. G.; Kaprelov, A. M. Disclination in an Elastic Sphere. *Philos. Mag. A* **1991**, *64*, 281−287.
(45) Johnson, C. L.; Snoeck, E.; Ezcurdia, M.; Rodriguez-Gonzalez, B.; Pastoriza-Santos, I.; Liz-Marzan, L. M.; Hytch, M. J. Effects of Elastic Anisotropy on Strain Distributions in Decahedral Gold Nanoparticles. *Nat. Mater.* **2008**, *7*, 120−124.
(46) Elechiguerra, J. L.; Reyes-Gasga, J.; Yacaman, M. J. The Role of Twinning in Shape Evolution of Anisotropic Noble Metal Nanostructures. *J. Mater. Chem.* **2006**, *16*, 3906−3919.
(47) Wu, H.-L.; Tsai, H.-R.; Hung, Y.-T.; Lao, K.-U.; Liao, C.-W.; Chung, P.-J.; Huang, J.-S.; Chen, I. C.; Huang, M. H. A Comparative Study of Gold Nanocubes, Octahedra, and Rhombic Dodecahedra as Highly Sensitive SERS Substrates. *Inorg. Chem.* **2011**, *50*, 8106−8111.
(48) Ikeda, K.; Suzuki, S.; Uosaki, K. Crystal Face Dependent Chemical Effects in Surface-Enhanced Raman Scattering at Atomically Defined Gold Facets. *Nano Lett.* **2011**, *11*, 1716−1722.
(49) Chiu, C.-Y.; Chung, P.-J.; Lao, K.-U.; Liao, C.-W.; Huang, M. H. Facet-Dependent Catalytic Activity of Gold Nanocubes, Octahedra, and Rhombic Dodecahedra toward 4-Nitroaniline Reduction. *J. Phys. Chem. C* **2012**, *116*, 23757−23763.
(50) Arenal, R.; Blase, X.; Loiseau, A. Boron-Nitride and Boron-Carbonitride Nanotubes: Synthesis, Characterization and Theory. *Adv. Phys.* **2010**, *59*, 101−179.
(51) Arenal, R. Low-Loss Studies on Metallic and Insulating Nanostructures Using a Monochromatic Electron Beam. *Microsc. Microanal.* **2011**, *17*, 768−769.
(52) Bosman, M.; Keast, V. J.; Watanabe, M.; Maaroof, A. I.; Cortie, M. B. Mapping Surface Plasmons at the Nanometre Scale with an Electron Beam. *Nanotechnology* **2007**, *18*, 165505.
(53) Arenal, R.; Henrard, L.; Roiban, L.; Ersen, O.; Burgin, J.; Tréguer-Delapierre, M. Local Plasmonic Studies on Individual Core-Shell Gold-Silver and Pure Gold Nano-Bipyramids. *J. Phys. Chem. C* **2014**, DOI: 10.1021/jp5066105.
(54) Jeanguillaume, C.; Colliex, C. Spectrum-Image: The Next Step in EELS Digital Acquisition and Processing. *Ultramicroscopy* **1989**, *28*, 252−257.
(55) Arenal, R.; de la Peña, F.; Stéphan, O.; Walls, M.; Tencé, M.; Loiseau, A.; Colliex, C. Extending the Analysis of EELS Spectrum-Imaging Data, from Elemental to Bond Mapping in Complex Nanostructures. *Ultramicroscopy* **2008**, *109*, 32−38.
(56) Myroshnychenko, V.; Nelayah, J.; Adamo, G.; Geuquet, N.; Rodríguez-Fernández, J.; Pastoriza-Santos, I.; MacDonald, K. F.; Henrard, L.; Liz-Marzán, L. M.; Zheludev, N. I.; Kociak, M.; García de Abajo, F. J. Plasmon Spectroscopy and Imaging of Individual Gold Nanodecahedra: A Combined Optical Microscopy, Cathodoluminescence, and Electron Energy-Loss Spectroscopy Study. *Nano Lett.* **2012**, *12*, 4172−4180.
(57) Álvarez-Puebla, R. A. Effects of the Excitation Wavelength on the SERS Spectrum. *J. Phys. Chem. Lett.* **2012**, *3*, 857−866.
(58) Hurst, S. J.; Lytton-Jean, A. K. R.; Mirkin, C. A. Maximizing DNA Loading on a Range of Gold Nanoparticle Sizes. *Anal. Chem.* **2006**, *78*, 8313−8318.
(59) Aslan, K.; Perez-Luna, V. H. Surface Modification of Colloidal Gold by Chemisorption of Alkanethiols in the Presence of a Nonionic Surfactant. *Langmuir* **2002**, *18*, 6059−6065.
(60) Krpetić, Ž.; Singh, I.; Su, W.; Guerrini, L.; Faulds, K.; Burley, G. A.; Graham, D. Directed Assembly of DNA-Functionalized Gold Nanoparticles Using Pyrrole−Imidazole Polyamides. *J. Am. Chem. Soc.* **2012**, *134*, 8356−8359.
(61) Jung, H. Y.; Park, Y.-K.; Park, S.; Kim, S. K. Surface Enhanced Raman Scattering from Layered Assemblies of Close-Packed Gold Nanoparticles. *Anal. Chim. Acta* **2007**, *602*, 236−243.
(62) Tetsassi Feugmo, C. G.; Liégeois, V. Analyzing the Vibrational Signatures of Thiophenol Adsorbed on Small Gold Clusters by DFT Calculations. *ChemPhysChem* **2013**, *14*, 1633−1645.
(63) Moskovits, M.; Suh, J. S. Surface Selection Rules for Surface-Enhanced Raman Spectroscopy: Calculations and Application to the Surface-Enhanced Raman Spectrum of Phthalazine on Silver. *J. Phys. Chem.* **1984**, *88*, 5526−5530.
(64) Moskovits, M.; DiLella, D. P.; Maynard, K. J. Surface Raman Spectroscopy of a Number of Cyclic Aromatic Molecules Adsorbed on Silver: Selection Rules and Molecular Reorientation. *Langmuir* **1988**, *4*, 67−76.
(65) Graf, C.; Vossen, D. L. J.; Imhof, A.; van Blaaderen, A. A General Method to Coat Colloidal Particles with Silica. *Langmuir* **2003**, *19*, 6693−6700.
(66) Guerrini, L.; Rodriguez-Loureiro, I.; Correa-Duarte, M. A.; Lee, Y. H.; Ling, X. Y.; Garcia de Abajo, F. J.; Alvarez-Puebla, R. A. Chemical Speciation of Heavy Metals by Surface-Enhanced Raman Scattering Spectroscopy: Identification and Quantification of Inorganic- and Methyl-Mercury in Water. *Nanoscale* **2014**, *6*, 8368−8375.
(67) Egerton, R. F. *Electron Energy-Loss Spectroscopy in the Electron Microscope*; Plenum: New York, 1996.